Towards Scalable Backscatter Sensor Mesh with Decodable Relay and Distributed Excitation

Jia Zhao
Simon Fraser University
BC, Canada
zhaojiaz@sfu.ca

Wei Gong
University of Science and Technology of China, China
weigong@ustc.edu.cn

Jiangchuan Liu
Simon Fraser University
BC, Canada
jcliu@cs.sfu.ca

ABSTRACT

Backscatter communication, in which data is conveyed through reflecting excitation signals, has been advocated as a promising green technology for Internet of Things (IoT). Existing backscatter solutions however are mostly *centralized*, relying on a single excitation source, typically within one hop. Though recent works have demonstrated the viability of multi-hop backscatter, the excitation signal remains centralized, which attenuates quickly and fundamentally limits the communication scope. For long-range and high-quality communication, distributed excitations are expected and also naturally available as ambient signals (WiFi, BLE, cellular, FM, light, sound, etc.), albeit not being explored for boosting nearby tags for relaying.

Given the existence of distributed excitation, a relay tag has to be *decodable*, i.e., be able to first decode its previous hop's information and then backscatter to the next hop with a boost from a nearby excitation whenever possible. In this paper, we present *DecRel*, a decodable tag relay solution towards a backscatter sensor mesh for universal and scalable deployment with distributed excitation. DecRel is also an innovative wireless sensor architecture for simultaneous sensing and relay. It incorporates a relay path that uses envelope detection for decoding, and a sensing path that converts its own sensor data into a baseband for amplitude-demodulation by the next hop tag's relay path. The two paths then backscatter their respective data to different frequencies to avoid interference. We have built a working DecRel tag prototype using FPGA, discrete components, and off-the-shelf analog devices. Our experiments show superior performance of DecRel as compared with the state-of-the-art non-decodable tag relay: specifically, a digital baseband's multi-hop throughput of up to 40Kbps (200x improvement), an analog baseband's equivalent multi-hop throughput of up to 768Kbps (3000x improvement), and a tag-to-tag distance of up to 4.8m (10x improvement) with a hop count of up to 6. DecRel tag consumes 337.9μW of power using IC design.

CCS CONCEPTS

• **Networks** → **Cyber-physical networks**; **Network architectures**; **Sensor networks**.

MobiSys '20, June 15–19, 2020, Toronto, ON, Canada

ACM ISBN 978-1-4503-7954-0/20/06…$15.00
https://doi.org/10.1145/3386901.3388942

KEYWORDS

Backscatter, Decodable Relay, Mesh Networks, Internet of Things

ACM Reference Format:
Jia Zhao, Wei Gong, and Jiangchuan Liu. 2020. Towards Scalable Backscatter Sensor Mesh with Decodable Relay and Distributed Excitation. In *The 18th Annual International Conference on Mobile Systems, Applications, and Services (MobiSys '20), June 15–19, 2020, Toronto, ON, Canada.* ACM, New York, NY, USA, 13 pages. https://doi.org/10.1145/3386901.3388942

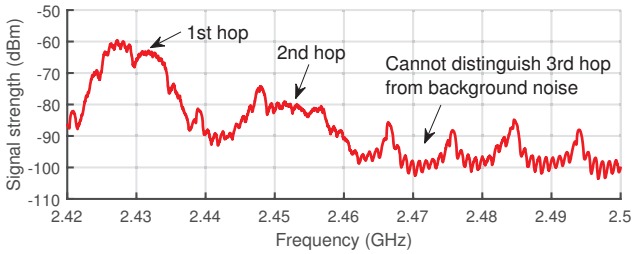

Figure 1: Attenuation of multi-hop backscatter signals using centralized excitation and non-decodable tag relay. Each tag forwards its previous hop tag signal to the next hop with a 20MHz frequency shift. Since each tag cannot decode its previous hop tag data, they can only use the first hop's excitation, which limits multi-hop backscatter communication scope.

1 INTRODUCTION

Building large-scale multi-hop sensor networks has to deal with two critical issues. **(i) Energy efficiency:** As the number of sensors is exploding, a large-scale sensor mesh needs low power and even battery-free connection solutions to push the limit of operational lifetime. **(ii) Scalability:** Sensors should enable the interconnection between each other as well as long-distance and high-performance relays, so that the network coverage can be significantly extended by simply increasing the number of sensors. Therefore, much effort has been made towards novel sensor architectures and efficient forwarding techniques [43–48].

Recently, low-power sensor design has advanced in a promising direction: RF-powered sensing devices [3, 6, 16, 23, 38], which use backscatter communication for sensor data transmission. The energy efficiency comes from the carrier and hardware power supply. A backscatter tag uses ambient signals (e.g., cellular, WiFi, Bluetooth, FM radio, visible light, and sound) as its carrier rather than proactively generate a carrier, hence eliminating the power-hungry high-frequency oscillators. A passive tag can also perform

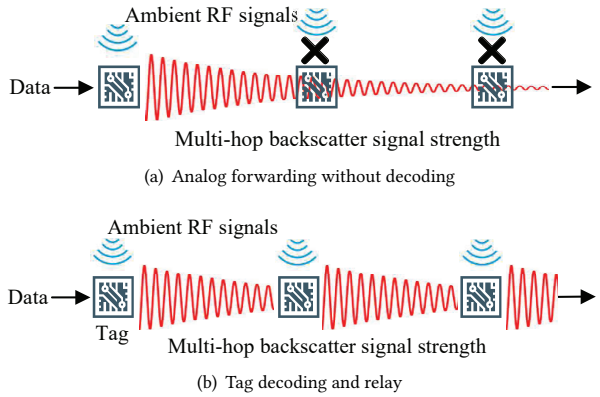

Figure 2: Different ways to use excitation in multi-hop backscatter communication: (a) non-decodable relay tags can only use 1st-hop's ambient signals; (b) improving multi-hop signal strength using ambient signals for each tag.

communication fully with the energy harvested from ambient electromagnetic or mechanical waves. Various backscatter-based sensor architectures have been proposed [23, 25, 33, 38, 55], enabling a wide range of realtime applications from scalar data sensing (temperature, humidity, light, etc) to multimedia data streaming (video, audio, and image). However, these designs all follow a single-hop mode, i.e., data transfer from a sensor to a sink, without relay communication that is necessary for sensor mesh networks. Multi-hop passive transmission can not only inherit such benefits of traditional multi-hop wireless networks as improving connectivity, extending coverage, enhancing robustness, and transforming power-consuming long links into efficient and flexible short links, but also develop an innovative and power-efficient networking framework for large-scale sensing.

Tag relay plays a key role in the change from single-hop backscatter communication to multi-hop backscatter networks. Prior work [30] demonstrates a multi-hop backscatter system that enables multiple backscatter tags to perform relay for each other. The sensing data can either be directly backscattered to the reader or be backscattered multiple times via multi-hop intermediate tags before the reception by the reader. This design enhances the robustness of backscatter networks when there is a poor channel condition for the direct path from a tag to the reader. Yet it is not well suited for a large-scale sensor mesh due to multi-hop signal attenuation as shown in Figure 1. Following the configurations in [30], we implement a three-hop backscatter system with an 802.11n WiFi excitation. Three tags are lined up as the route order, with a distance of 10cm between any two consecutive hop tags. Each tag forwards its previous hop tag signal to the next hop with a 20MHz frequency shift. As shown in Figure 1, there is a rapid signal attenuation as hop count increases, and the 3rd hop signal is too weak to be distinguished from noises.

Multi-hop signal attenuation in Figure 1 can be ascribed to the availability of a centralized excitation only. As shown in Figure 2(a), multiple tags can only use the first hop ambient signal. Such an excitation mode is determined by non-decodable tag relay, where a tag can only reflect the pre-hop backscatter signal entirely without

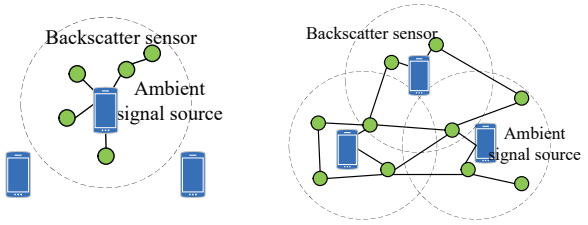

(a) Centralized excitation and non-decodable relay (b) Distributed excitation and decodable relay

Figure 3: Comparison of backscatter sensor networks using: (a) centralized excitation and non-decodable relay; and (b) distributed excitation and decodable relay.

any change or directly use this signal as its excitation. When a post-hop tag moves away from this excitation, its backscattered signal will attenuate rapidly due to multiple times of reflection, and fundamentally limit hop count, tag-to-tag distance and multi-hop throughput.

This motivates us to change the excitation mode. We are inspired by the ubiquitous presence of such devices as smartphones, PCs, wearables, APs, and illuminators, all of which can potentially work as excitation sources in either indoor or outdoor environments. They naturally exist in a large-scale and densely distributed manner, potentially serving as excitation signals almost anytime and anywhere. A distributed excitation mode can fully utilize any already existing signals to improve multi-hop communication quality without extra costs, as illustrated in Figure 2. The prerequisite is to enable a decodable tag relay, i.e., decoding the pre-hop data and backscattering it to the next hop. As shown in Figure 3, decodable relay and distributed excitation can largely extend the sensor network coverage as compared to the centralized mode and bring desirable multi-hop merits (e.g., low power, high throughput, backup paths, robustness, and even multipath transmission over a mesh). Yet to realize the idea, we need to overcome the following obstacles.

- **Baseband design.** A relay tag should be able to decode a wide range of data, from digital data to analog data, and from scalar data to multimedia data. Since all the data is presented with pre-hop baseband signal, we need a deliberate baseband circuit design to reduce the complexity of decoding.
- **Poor signal strength.** Backscattered signal strength is usually very weak. For example, Figure 1 shows that even the first hop backscattered signal is less than -60dBm, and the signal attenuates fast as exciter-to-tag distance increases. Such a signal strength is difficult for envelope detection.
- **Simultaneous sensing and relay.** While tags need to do relay for each other, their own sensing data transmission should not be interrupted by the relay. This requires concurrent transmission when a relay request comes along with an ongoing sensing task.
- **Tag relay in different conditions.** Tag relay should provide multiple options. For example, realtime temperature sensing and acoustic sensing need different transmission rates, which may be obtained using different forwarding circuits. We should also consider the mobility that sensors can have time-variant relative position. When a tag performs relay communication, it needs to

select a proper forwarding mode according to the distance from its previous hop tag.

In this paper, we present DecRel for scalable multi-hop backscatter communication. DecRel is not only a decodable tag relay framework but also an innovative sensor architecture. Figure 4 shows a DecRel sensor that performs simultaneous sensing and relay. Specifically, we make the following technical designs to address our challenges.

- **Sensing frontend and baseband modulation.** We introduce a data processing path, called *sensing path*, to generate baseband signals which are suited for amplitude demodulation. It can generate either a BPSK-based digital baseband for scalar data sensing or a PWM-based analog baseband for high-bitrate multimedia data sensing.
- **Envelope detection.** We design another data processing path, called *relay path*, to enable a tag to decode its previous hop tag's baseband signal. We use a double diode detection circuit as our envelope detector, which greatly increases the sensitivity and dynamic range of amplitude demodulation. An aggregation node is also introduced to assist a tag for the envelope detection of a weak backscattered signal.
- **Backscatter with two different frequency shifts.** We use two frequency-shifted clock signals, with which a tag can backscatter the same excitation signal to two different frequencies for sensing path and relay path, respectively, and hence incurring no interference between the two paths.
- **Tag reconfiguration.** Our tag is reconfigurable through sending a wireless control message. The controlled operations include switching on/off digital or analog baseband circuits, selecting different frequency-shifted clock, and selecting between decodable or non-decodable relay circuits (which also offers compatibility with previous systems).

We have built a tag prototype using FPGA, discrete components, and off-the-shelf analog devices. We measure the power consumption of our prototype PCB and optimize it to 337.9μW using IC design. We evaluate the communication performance via field experiments. Compared with the state-of-the-art non-decodable tag relay, DecRel can achieve a digital baseband's multi-hop throughput of up to 40Kbps (200x improvement), an analog baseband's equivalent multi-hop throughput of up to 768Kbps (3000x improvement), and a tag-to-tag distance of up to 4.8m (10x improvement) with a hop count of up to 6.

2 DESIGN

We introduce the main components in the architecture of a DecRel sensor tag and how it works in a mesh network, as shown in Figure 4, which highlights the sensing and relay paths within a backscatter tag. For each path, we next give the details including baseband generation, modulation, backscatter communication and demodulation. The key is to understand the correlation between the two paths, i.e., how the data from pre-hop sensing path can be decoded and forwarded by post-hop relay path.

2.1 Sensing Path

2.1.1 Sensing Frontend. Realtime sensing applications usually have a large variation of data rate. For example, off-the-shelf temperature

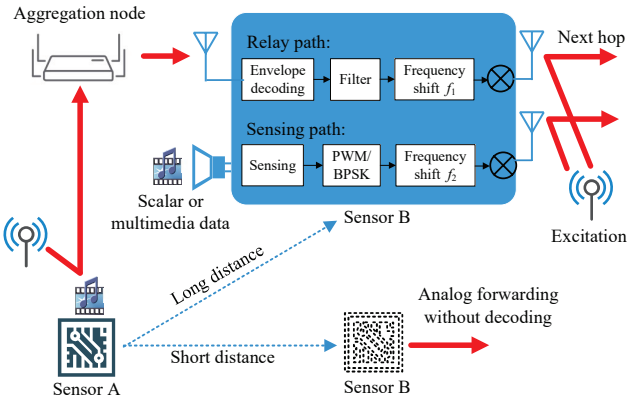

Figure 4: Simutaneous sensing and relay in multi-hop backscatter sensor mesh.

sensors use tens of bits to represent thermal information, which can be transmitted at a data rate of tens of kilobits per second; HD video streaming however needs tens to hundreds of megabits per second. To be compatible with both low-bitrate scalar data and high-bitrate multimedia data, we design two types of sensing frondend.

The digital sensing frontend is shown in Figure 5(a). It consists of external sensors and readout devices that can convert sensor output into a bit stream for the subsequent modulation. The readout devices can be an ADC or drive program written with hardware description language. The external sensors are flexible to be added to or removed from the tag hardware. This digital sensing frontend fits scalar data acquisition.

The analog sensing frontend is shown in Figure 5(b). It consists of discrete components and analog sensing components, such as thermistor, photoresistor and electret microphone, corresponding to the analog readout for temperature, light and sound, respectively. The analog sensing frontend fits high-bitrate multimedia data acquisition. We employ analog sensing frontend for two reasons. **(i) Low power transmission**, as demonstrated in previous studies for backscattering audio and HD video [25, 33, 38]. **(ii) Lightweight and efficient transmission.** Conventional sensor transmission is built over computing capability, especially for multimedia sensors that use a set of power-hungry components for digitizing, encoding and streaming. For example, off-the-shelf camera drones integrate a small-scale video streaming server to connect to its client APPs on PCs or smart devices [1]. Such a transmission mode usually uses a single-board computer (e.g., Raspberry Pi [2]) that integrates CPU, memory, storage, I/O, wireless adapter, etc, running an OS or SDK. Since today's applications have already decoupled sending from computing, the power-hungry components, such as ADC, DSP, codec, microprocessors, and even wireless adapters, should be removed from a wireless sensor node, so as to keep it light-weight and working efficiently.

2.1.2 Baseband Modulation. The modulation in Figure 5 converts the sensing data into a baseband signal. Given two types of sensing frontend, DecRel tags need to use different modulation approaches to generate digital baseband and analog baseband, respectively. The digital baseband can work with diverse state-of-the-art sensors,

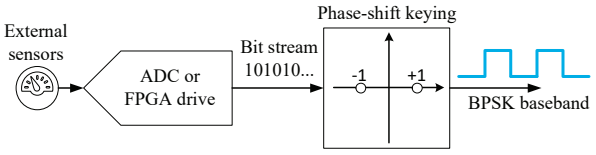

(a) Digital sensing and baseband using BPSK

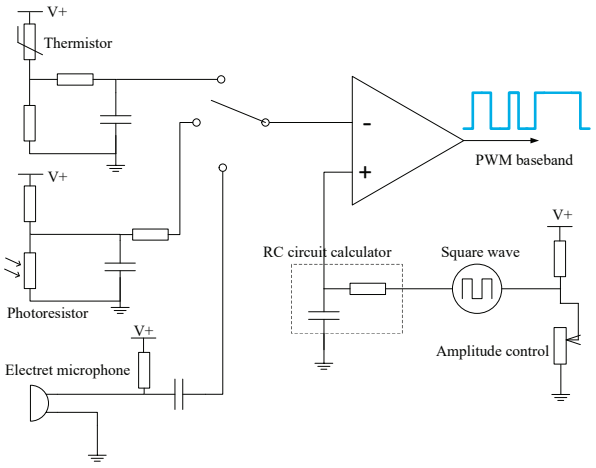

(b) Analog sensing and baseband using PWM

Figure 5: Two types of sensing frontend and baseband modulation in our design for digital data and analog data, respectively. (a) Digital baseband signal is generated using off-the-shelf sensors and BPSK modulation. (b) Analog baseband signal signal is generated using analog devices and discrete components.

while the analog baseband achieves high throughput for multimedia signal transmission.

Figure 5(a) shows that the digital baseband circuit converts a bit stream into fixed-length binary voltage amplitudes for BPSK modulation (using an XOR operation of binary amplitudes and a 10MHz square wave, as will be introduced in Subsection 3.2.1). Figure 6 shows an example of digital baseband signal that is generated for BPSK modulation in Figure 5(a). The baseband is converted from a bit stream that repeatedly sends data '10110'. There are consecutive voltage levels with a fixed length, where each high level represents data '1' and each low level represents data '0'. Digital baseband also enables our backscatter tag to work with commodity radios, such as WiFi and Bluetooth.

For analog baseband, we use the pulse width modulation circuit as shown in Figure 5(b), which includes a voltage comparator, an RC circuit calculator and a sampling clock. The non-inverting input of the comparator is connected to the output of the RC circuit, which generates a periodic triangular wave. The inverting input of the comparator is connected to the output of the analog sensing frontend. For an analog signal, this modulation circuit generates a baseband signal that uses each pulse width to represent the analog during each triangular wave sampling period. Figure 7 shows a trace of signals generated by the sensing and modulation circuits in Figure 5(b). Figure 7(a) shows the time-domain waveform of

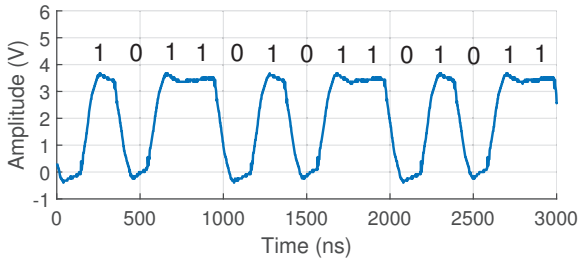

Figure 6: Binary amplitude digital baseband for BPSK modulation in Figure 5(a).

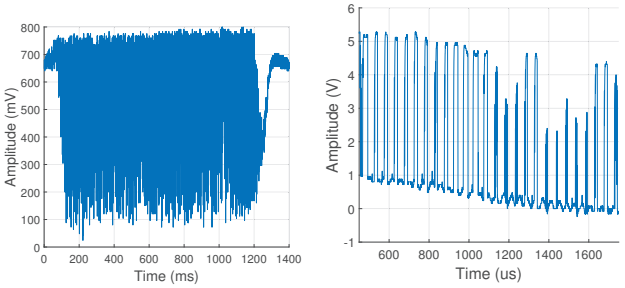

(a) Audio analog signal (b) 50KHz PWM baseband

Figure 7: Analog baseband signal using PWM in Figure 5(b).

an audio signal that is captured from the analog sensing frontend. Figure 7(b) shows a part of the baseband signal from the PWM circuit with a sample rate of 50KHz. We can see that the pulse width varies in Figure 7(b), where the wider a pulse is, the smaller its corresponding analog amplitude is. The drift of the PWM signal amplitude is brought by the noise of triangular wave sampling circuits and can be cancelled using a voltage threshold filter.

As shown in Figure 6 and Figure 7(b), both digital and analog baseband signals employ the simplest amplitude information (high or low voltage level), which can be easily detected by a diode envelope detector. The baseband design above is the key for decodable tag relay. In Subsection 2.2, we will introduce how a tag's baseband signal is decoded and forwarded along its next hop tag's relay path.

2.2 Relay Path

2.2.1 Envelope Detection. The decoding function in our design is not to recover the original data collected by the sensing frontend (e.g., a bit stream by the digital sensing frontend or a time-domain waveform by the analog sensing frontend), but to demodulate the pre-hop tag's baseband signals (e.g., Figure 6 and Figure 7(b), where a baseband signal carries necessary information for recovering the original data in that duration). Our tag directly embeds a decoded baseband after filtering onto an excitation signal for backscattering. During multi-hop communication, the tags do not change the baseband signal of the first hop tag, and just forward the same signal hop by hop.

A key step is to obtain the correct baseband. This is guaranteed by the previous hop tag's baseband form and the current hop tag's envelope detection. As we have discussed in Subsection 2.1, a digital

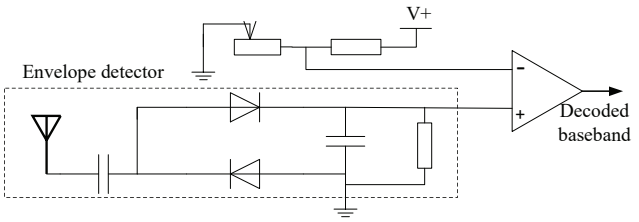

Figure 8: Envelope detector circuit for previous hop tag baseband detection.

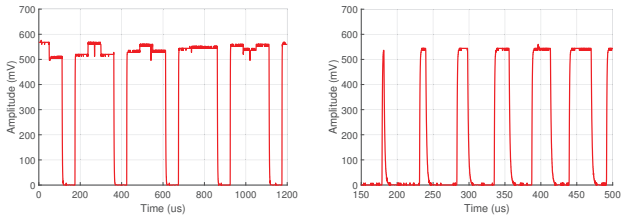

(a) BPSK signal detected by envelope detector

(b) Pulse width modulation signal with 48KHz sample rate detected by envelope detector

Figure 9: Our tag's envelope detector output for (a) digital baseband signal using BPSK; and (b) analog baseband signal using PWM.

or analog baseband from the previous hop tag's sensing path can directly modulate a carrier with time-variant amplitudes. Hence, we employ an amplitude demodulation in our tag with envelope detection. Our envelope detector design is shown in Figure 8, which consists of a double diode circuit, an omnidirectional antenna and discrete components. The two diodes have a reverse connection and can detect an AC signal positively and negatively, hence significantly increasing the sensitivity and dynamic range of detection compared to a basic single diode detector. To illustrate how the envelope detector works, we record its output as a trace. Figure 9(a) shows the detected envelope for a digital baseband that repeatedly sends data '1'. Figure 9(b) shows the detected envelope for an analog baseband that represents a part of an analog signal using pulse width modulation at a 48KHz sample rate. Subsection 3.1.1 will discuss the implementation of this design with off-the-shelf analog devices.

2.2.2 Correlation with Sensing Path. While a tag's relay path is independent of its own sensing path, it is closely correlated with its previous hop tag's sensing path. When performing relay, a tag recovers the baseband signal with amplitude demodulation. Such a design brings three advantages. First, the decoding circuit of the relay path is simplified and consumes low power. Since the baseband signal can be directly used for amplitude modulation, the tag decoding function can simply use an envelope detector built with low-power analog devices and discrete components. Unlike other complex demodulation techniques, envelope detection does not use high-frequency oscillators and external power supply, hence reducing the power consumption. Second, the relay path eliminates a specific baseband circuit and becomes lightweight as compared to the sensing path circuits in Figure 5. Third, amplitude demodulation also enables a sensing path to employ the analog baseband circuit, which achieves low power and high throughput simultaneously.

2.2.3 Aggregation Node. An aggregation node assists a tag to decode when doing relay. It is implemented currently to serve our goals but could be eliminated in a future design. This is because its decoding functions can be replaced using a low-power ADC [61] or an on-tag multi-antenna decoding solution [18] (where the only concern is a trade-off between throughput and tag-to-tag distance). The main reason for using an aggregation node is that the pre-hop backscatter signal strength is usually too weak to be detected by a post-hop tag's envelope detector, especially when there is a long distance between the two tags. The aggregation node can first demodulate a tag's baseband signal and then broadcast it wirelessly (with limited range and controlled power). This proactive transmission uses single-tone carrier and amplitude modulation, which provide sufficient signal strength for a nearby tag's envelope detection. Besides assisting the decoding, the aggregation node can also be used to send notification and control messages to its nearby tags, just like a conventional aggregation node or base station in wireless mesh networks.

2.3 Simultaneous Backscatter for Two Paths

A backscatter tag needs two steps to send its data out. The first is tag modulation, which is to generate a signal with time-variant amplitude to change antenna impedance. The second is to use the antenna with time-variant impedance to reflect or absorb an excitation signal. Both sensing path and relay path perform backscatter communication. To avoid their mutual interference, we need a specific design. Previous works [9, 10, 33] use frequency shift to cancel the interference between the excitation signal and backscattered signal. To tackle our problem, we use two frequency-shifted clock signals that can backscatter an excitation signal to two different frequencies for sensing data and relay data, respectively. Figure 10 shows the experiment results of simultaneous sensing and relay during multi-hop backscatter communication. Figure 10(a) shows that the first hop tag backscatters its data to a center frequency with a 10MHz frequency shift from its excitation signal. The second hop tag's relay path uses a 10MHz frequency shift, while its sensing path uses a 20MHz frequency shift. There is no interference between the two paths as shown in Figure 10(b). The control messages are sent to notify a tag to perform sensing or relaying, or both simultaneously. The tag detects and follows the control message to switch on or off the corresponding frequency-shifted clocks. The implementation of frequency shift will be introduced in Subsection 3.2.2.

2.4 Reader Demodulation

DecRel's reader first uses coherent demodulation to remove the single-tone carrier. As shown in Figure 10(b), we can obtain a 10MHz signal for relay data and a 20MHz signal for sensing data after removing the excitation carrier. Subsection 3.2.1 presents a practical logic circuit to implement the phase modulation, where a tag uses a 10MHz or 20MHz square wave to XOR a baseband signal. The binary amplitude values (i.e., voltage level in pulse duration and pulse interval) in a baseband are modulated with a 180° phase offset. Hence, we use a quadrature phase discrimination to extract

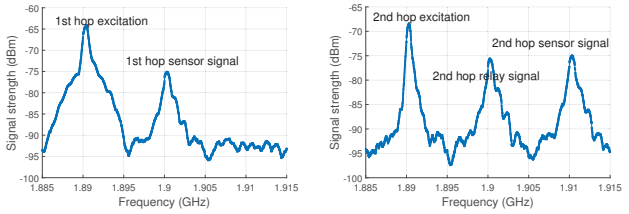

(a) The first hop tag's frequency spectrum

(b) The second hop tag's frequency spectrum

Figure 10: Two hop tags frequency spectrum. Fig. 10(b) shows that: the 2nd hop tag's relay signal strength does not decrease compared to the 1st hop tag signal in Fig. 10(a); and the 2nd hop tag can perform backscatter communication for simultaneous sensing and relaying with different frequency shifts.

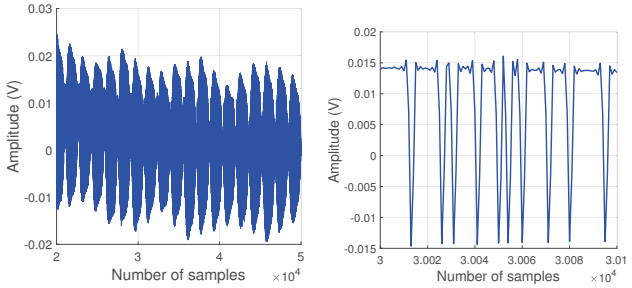

(a) Demodulated signal with 30000 consecutive samples

(b) A fine-grained view of pulses with varying width

Figure 11: Demodulated backscatter signal that represents analog data with pulse width.

the baseband from the phase-modulated 10MHz or 20MHz signal. Figure 11 shows a trace of the demodulated backscatter signal with time-variant pulse widths.

2.5 Mobility and Tag Reconfiguration

Our design also provides two available tag relay modes: decodable tag relaying and analog forwarding. This considers that individual tags may have mobility in a practical deployment and a tag-to-tag distance can be time-variant. Such a design offers flexibility for a tag to select the efficient relay approach. As shown in Figure 4, when there is a long distance between two tags, the second hop tag can maintain high-quality relay communication using the decoding function. When there is a short distance between two tags, the second hop tag can be reconfigured to use analog forwarding, which can be simply achieved using a frequency shift with very low power consumption. We can also reconfigure a tag with other operations, such as switching on/off digital or analog baseband circuits and selecting different clock signals for a frequency shift. All the reconfigurations can be performed over a wireless connection, and their implementation is introduced in Subsection 3.2.3.

3 IMPLEMENTATION

In this section, we implement our design using both prototype and IC design. We build a prototype PCB of our decodable backscatter tag as shown in Figure 12 using an FPGA, discrete components, and off-the-shelf IC devices. The prototype uses customized analog circuits and FPGA digital circuits to provide the functionality in Section 2. We also build a prototype of the multi-hop backscatter communication system with our tags and commodity radios. In addition to the PCB-level implementation, we use an IC design for power consumption analysis and optimization.

3.1 Analog Circuits

3.1.1 Analog Circuits in Relay Path. The envelope detection circuit follows the design in Figure 8. Its essential component is a diode detector. We use a P2D SCR thyristor as the diode detector, which is equivalent to a double diode detection circuit. The output of the diode detector is connected to an RC filter that consists of a 10kΩ resistor and a 1nF capacitor. In Figure 8, the envelope detection circuit also uses a variable resistor that determines the discrimination voltage of the comparator. We set a threshold voltage of 0.3V to discriminate between high and low voltages, so as to cancel noise and step up voltage for the follow-up FPGA modules. We use voltage comparator TLV3501 with 4.5ns propagation delay and a sliding rheostat circuit for tuning the threshold voltage. The operating frequency of our envelope detector can be up to 3200MHz. The antenna of our envelope detector is vertically polarized with a gain of 3dBi and a frequency range from 824MHZ to 960MHz and from 1710MHz to 1990MHz.

3.1.2 Analog Circuits in Sensing Path. The sensing path's analog circuits follow the design in Figure 5. For the digital sensing frontend, we reserve enough input/output FPGA pins on the tag prototype PCB to be connected to external off-the-shelf sensors. For the analog sensing frontend, we build the customized circuits with discrete components and analog devices, as shown in Figure 5(b). We use three types of analog sensing devices, including thermistor, photoresistor and electret microphone. The output of the analog sensing frontend is connected to a PWM baseband circuit that consists of a voltage comparator and an RC calculator. We use voltage comparator TLV3501 and build the calculator circuit with a 10kΩ resistor and a 100nF capacitor.

3.2 FPGA Circuits

3.2.1 Tag Modulation Circuits. We implement all the digital logic circuits in a XILINX Spartan XC3S500E-4PQ208 FPGA. We use Verilog to specify the logic functions in FPGA. As introduced in Subsection 2.3, the tag modulation converts a baseband signal into an antenna impedance control signal, which is the key for a tag to perform backscatter communication. Figure 14 shows the implementation of our tag modulation circuits for analog and digital baseband signals, respectively. As shown in Figure 14(a), the tag modulation for analog baseband is performed using an XOR operation. We XOR an analog baseband signal and a frequency-shifted clock signal to generate the output signal that directly controls an ADG902 RF switch. The output signal has the same frequency as the frequency-shifted clock signal, while its phase is time-variant along with the PWM baseband. The output signal is of 0° phase if there is a pulse of the PWM signal, and of 180° phase if there is a pulse interval. Figure 14(b) shows the tag modulation circuits

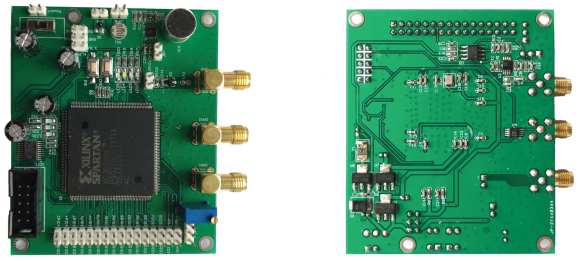

Figure 12: Prototype PCB of DecRel tag.

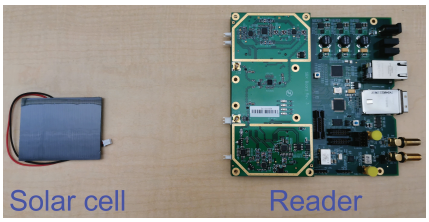

Figure 13: Reader and external power supply for tags.

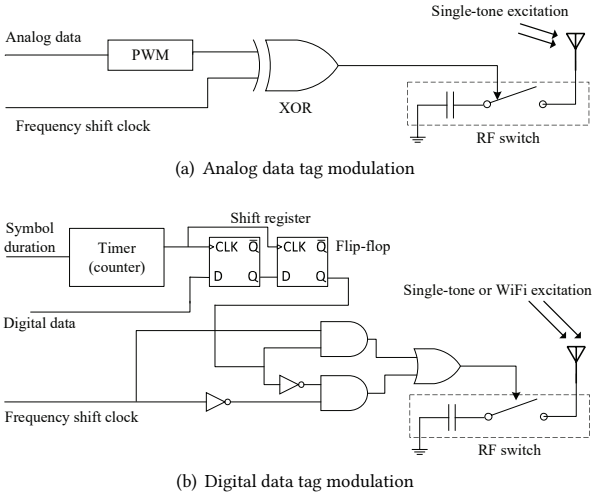

Figure 14: FPGA circuits for (a) analog data tag modulation; and (b) digital data tag modulation.

for digital baseband signals. The input digital data is a bit stream. We need to specify a fixed duration of high or low voltage for each data bit. We use a counter block and tune its threshold to satisfy the symbol duration. For single-tone excitation, the symbol duration uses the pulse width of envelope detection. When using WiFi excitation, we set the symbol duration to be an 802.11b bit or four 802.11g/n OFDM symbols, as in [10, 26]. For each counting cycle, the counter outputs '1' if it reaches the threshold, and '0' otherwise. The counter's output signal then enables a shift register to output only one bit for each symbol duration. The modulation outputs a frequency-shifted signal of 0° phase if the register outputs '1', and otherwise a 180° phase. Because our tag cannot decode a WiFi signal, WiFi excitation can only be used for the last hop tag, and in this case the reader should be a WiFi device. DecRel's tag modulation uses the positive edge of the first detected pulse (whose power consumption is included in the envelope detector of DecRel tag PCB) to synchronize to a single-tone excitation signal, and uses an external power amplifier detector (a 40mW AD8313 device, which does not count toward DecRel tag's PCB power consumption) to synchronize to the beginning of WiFi excitation packets.

3.2.2 Frequency-Shifted Clock Selection. As discussed in Subsection 2.3, DecRel's sensing path and relay path can backscatter an excitation signal to two different frequencies, both of which are away from the excitation frequency and thus do not impact each other. This enables a tag to perform sensing and relaying simultaneously. To implement such frequency shifts, a tag need two different clock signals for the two paths and a clock selection mechanism.

We use XC3S500E FPGA's internal 50MHz clock and the Verilog code for frequency division to generate a 10MHz and a 20MHz clocks, respectively. Clock selection can be configured with a 1-input 2-channel multiplexer. Figure 15 shows the associated FPGA circuit built with logic gates. For example, the relay path selects 10MHz frequency shift if SEL1 inputs '0', and selects 20MHz frequency shift otherwise. The selection ports SEL1 and SEL2 can be reconfigured once the tag receives a control message and its implementation will be introduced in Subsection 3.2.3. This control mechanism also guarantees that SEL1≠SEL2 if a tag's sensing path and relay path are switched on simultaneously.

3.2.3 Tag Reconfiguration Control. DecRel tags can be reconfigured over wireless connections from their nearby aggregation nodes. An aggregation node first broadcasts an 8-bit control message with a BPSK-modulated single-tone carrier. The broadcasting process follows the same way as the aggregation node forwarding in Subsection 2.2.3, so that a tag can use its envelope detector to recover the 8-bit message. Figure 16 shows the FPGA circuits that can interpret the control message and switch on/off the corresponding circuit modules. The 8-bit message is input into a shift register. The first three bits are used to specify a target tag's ID. Each tag has it own ID-matching circuit, which is unique and built with logic gates. When matching up with the target ID, the ID-matching circuit will output '1' to enable the follow-up configurations, and '0' to ignore the message otherwise. The other bits are used to switch between two relay modes, select baseband circuits, or select frequency-shifted clocks. DecRel tags can also be controlled to switch between decodable relay and analog forwarding. As shown in Figure 16, when Q3 outputs '1' and Q4 outputs '0' at the same time, the tag will switch on the analog forwarding mode.

3.3 Other Nodes

We implement our backscatter reader, excitation sources, and aggregation nodes with USRP N210 software-defined radio devices. The WiFi excitation and receiver use Qualcomm AR938x devices. The excitation uses RFMAX S9028PCR antenna with an 8.5 dBic gain. The reader and aggregation nodes use MTI 6.5 dBic MT-242025/TRH/A antennas. To deal with the interference among multi-hop tags, the excitation and aggregation nodes use different carrier center frequencies. For example, when the excitation uses 2.4GHz frequency band, the aggregation node will use 900MHz carrier. To examine

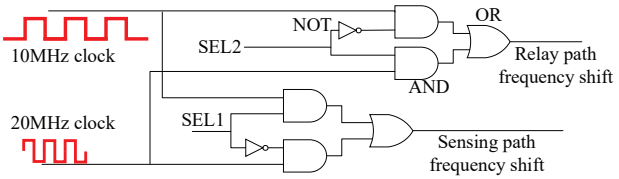

Figure 15: Frequency shift selection for sensing path and relay path.

hop count, tag-to-tag distance and multi-hop communication range, we change the positions of DecRel tags, the aggregation nodes and the reader with the following topology: DecRel tags and the reader are lined up by following the route order; The aggregation node is placed at a distance of up to 1m from a DecRel tag, which is determined by the sensitivity of our envelope detector. When measuring tag-to-tag distances, we use two tags and increase their distance from 1.2m to 4.8m. When measuring how hop count impacts the bit error rate, we locate tags with a fixed tag-to-tag distance (up to 2m), and increase the number of tags. To measure the last hop tag-to-reader distance, we fix the positions of the tags and aggregation nodes, and move the reader to increase the last hop distance from 1m to 12m for WiFi excitation and from 1m to 5m for single-tone excitation, respectively.

3.4 PCB and IC Power Measurement

The PCB implementation of our tag is used only to verify the functions in our design and demonstrate the signal quality and communication range. To measure the power consumption of DecRel tag PCB, we use Monsoon Power Monitor FTA22D [56]. The idle state consumes 107.3mW and the working state consumes 273.5mW on average. This power can be supplied by a solar panel shown in Figure 13. To further optimize the power consumption, we implement and simulate our design in an IC design platform: the analog components are implemented and evaluated using Cadence IC6.17 Virtuoso [57] and a TSMC 65nm CMOS Low Power technology library [58]; the digital components are synthesized using the Xilinx XPower analysis tool [59]. Table 1 compares IC design with PCB power consumption. A 20MHz oscillator consumes 317.5μW. The PWM baseband circuit consumes 4.3μW. The envelope detection circuit consumes 6.1μW. The power consumption of digital components does not exceed 10μW though it varies due to the selection of different baseband and modulation circuits. Therefore, the total power consumption of our tag is up to 337.9μW. Compared with previous non-decodable relay design in X-Tandem [30], DecRel largely reduces the power consumption of the frequency shift module, because we have developed the lightweight frequency division circuits rather than use a clock management IP core.

4 EVALUATION

This section evaluates the performance of DecRel with different configurations including digital baseband circuits, analog baseband circuits, and simultaneous sensing and relay. To compare DecRel with the previous systems using non-decodable tag relay, we record received signal strength indicator (RSSI), bit error rate (BER), multi-hop throughput, and signal-to-noise ratio (SNR). We also examine

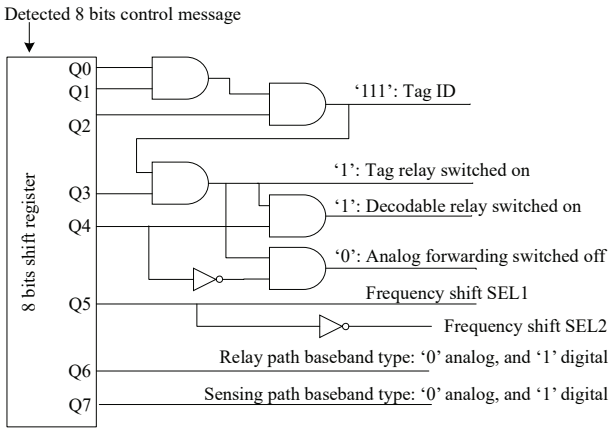

Figure 16: FPGA circuits for intepreting the control message and switching on or off different tag configurations.

Table 1: Comparison of PCB and IC power consumption

Impl.	Component power consumption				Total
	Oscillator	PWM	Envelope detector	Digital core	
PCB (Benchmark)	64.2mW	28.6mW	33.5mW	147.2mW	273.5 mW
IC	317.5μW	4.3μW	6.1μW	10.0μW	337.9 μW

multi-hop communication range and tag-to-tag distance, which directly impact the network scale.

4.1 Performance of DecRel with Digital Baseband and Modulation Circuits

The first experiment is conducted to evaluate the performance of DecRel when using digital baseband and digital data modulation circuits. We compare DecRel with X-Tandem [30], which is the prior work on multi-hop backscatter communication. X-Tandem tags use digital modulation and WiFi excitation signals. As we have introduced in Subsection 3.2, our implementation of DecRel tag can use either a WiFi signal or a single-tone signal as the excitation. As such, we configure the last hop tag to use WiFi excitation for the comparison of DecRel and X-Tandem. In addition, we also examine the performance of using single-tone excitation and WiFi excitation, respectively, with increasing tag-to-tag distance.

4.1.1 Hop Count, RSSI,BER and Throughput. We first implement a multi-hop system to examine how bit error rate changes with hop count. Table 2 shows that, given a tag-to-tag distance of 1m, the BER degrades from 0.037 to 0.185 as hop count increases from 2 to 6. To examine how multi-hop backscatter communication quality changes with the distance between the last hop tag and the backscatter reader, we use the following setup by referring to [30]: A two-hop backscatter system is deployed in an indoor environment; The tag-to-tag distance is 0.1m for X-Tandem, and 1m for

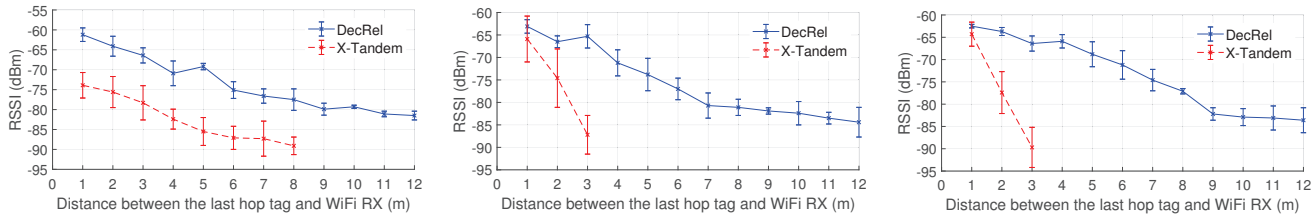

(a) 802.11b 1Mbps (b) 802.11g 6Mbps (c) 802.11n 6.5Mbps

Figure 17: The last hop backscattered signal strength across the distance between the last hop tag and WiFi receiver: DecRel outperforms X-Tandem in both communication range and signal quality for different excitation specifications.

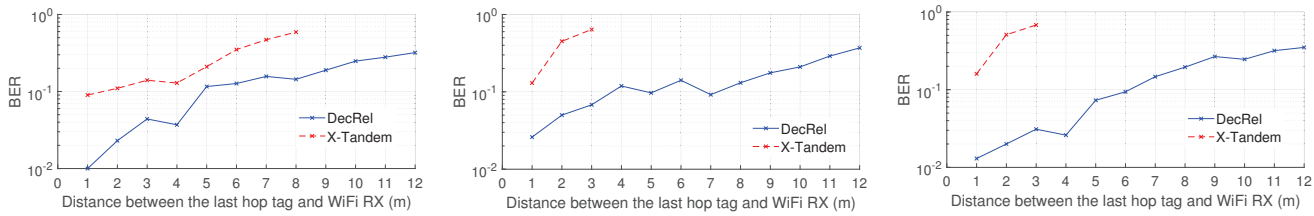

(a) 802.11b 1Mbps (b) 802.11g 6Mbps (c) 802.11n 6.5Mbps

Figure 18: The last hop backscattered signal bit error rate across the distance between the last hop tag and WiFi receiver: DecRel achieves better BER than X-Tandem for different excitation specifications.

Table 2: Bit error rate across hop count

Tag-to-tag	Bit error rate				
	2 hops	3 hops	4 hops	5 hops	6 hops
1 m	0.037	0.081	0.116	0.151	0.185
2 m	0.066	0.154	0.221	0.284	0.341

DecRel. At the beginning, the reader is placed at a distance of 1m from the second hop tag. Then we move the reader to increase the distance between the second hop tag and the reader. We use three types of WiFi excitation signals, including 802.11b 1Mbps, 802.11g 6Mbps, and 802.11n 6.5Mbps. Since these signals have different symbol durations, we need to reconfigure the counter of the tag modulation circuit for digital data in Figure 14(b). DecRel's first hop tag uses single-tone excitation, and its second hop tag uses WiFi excitation.

Figure 17 shows the last hop backscattered signal strength across the last hop distance. We can see that the signal strength decreases with the distance for both DecRel and X-Tandem in all the three cases. As shown in Figure 17(a), for an 802.11b 1Mbps excitation, DecRel's last hop signal strength is around -60dBm when there is a distance of 1m from the last hop tag to the WiFi receiver. The signal strength decreases to below -80dBm when the distance increases to 12m. For all the three types of WiFi excitation, DecRel outperforms X-Tandem in both the last hop signal strength and the communication range. When the distance between the last hop tag and the WiFi receiver is beyond 3m, the RSSI of DecRel is about 10dBm higher than that of X-Tandem in all the three sub-figures. The reason is that DecRel's last hop backscattered signal strength is not affected by previous hops, but determined by its own excitation. Therefore, multi-hop attenuation does not noticeably affect DecRel.

Figure 18 shows the bit error rate of the last hop backscattered signal across the last hop distance. Figure 19 shows how the multi-hop throughput changes with the the last hop distance. Our results show that DecRel also outperforms X-Tandem for all the three types of WiFi excitation. In particular, when the WiFi receiver is 1m away from the last hop tag, DecRel achieves a multi-hop throughput of 35.1Kbps, 32.6Kbps, and 33.0Kbps for 802.11b 1Mbps, 802.11g 6Mbps, and 802.11n 6.5Mbps, respectively. It is about 150x higher than that can be achieved by X-Tandem. When the last hop distance increases to 12m, DecRel can achieve a multi-hop throughput of 9.1Kbps using an 802.11n 6.5Mbps excitation. These results clearly demonstrate the backscattered signal strength improvement of DecRel's last hop. Specifically, X-Tandem's last hop communication uses its previous hop backscatter signal as excitation. As illustrated in Figure 2(a), severe signal attenuation happens to the analog forwarding mode in X-Tandem and directly leads to the limitations on multi-hop throughput. In contrast, DecRel's last hop communication uses a nearby excitation and hence achieves much better signal strength and throughput.

Figure 20 shows the performance of DecRel using WiFi excitation and single-tone excitation, respectively, for the last hop backscatter communication. For single-tone excitation, we use a USRP N210 device as the reader. The tag-to-tag distance is still fixed to 1m. As the distance between the last hop tag and the reader increases, there is a downward trend of the last hop signal strength when working with the single-tone excitation signal, as shown in Figure 20(a). The last hop tag using single-tone excitation has a signal strength of about -70dBm at a 1m distance, and decreases to below -85dBm when the distance increases to 5m. Figure 20(b) shows that the bit error rate of the single-tone case also increases with the last hop distance. The WiFi case outperforms the single-tone case in RSSI, BER, and the last hop distance. Although the peak throughput of

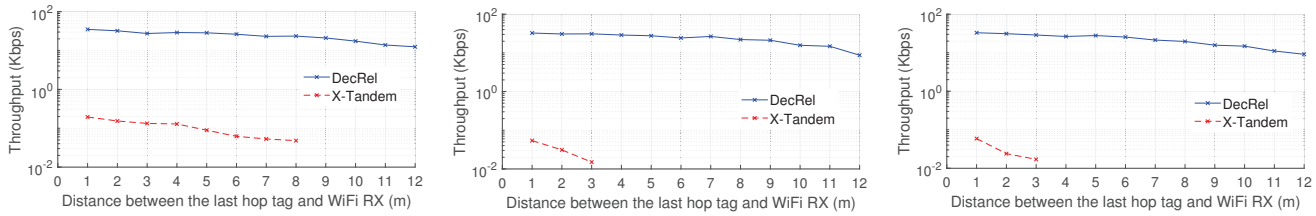

(a) 802.11b 1Mbps (b) 802.11g 6Mbps (c) 802.11n 6.5Mbps

Figure 19: The last hop backscattered signal throughput across the distance between the last hop tag and WiFi receiver: the multi-hop throughput of DecRel is up to 35.1Kbps for WiFi excitation and 150x higher than that of X-Tandem.

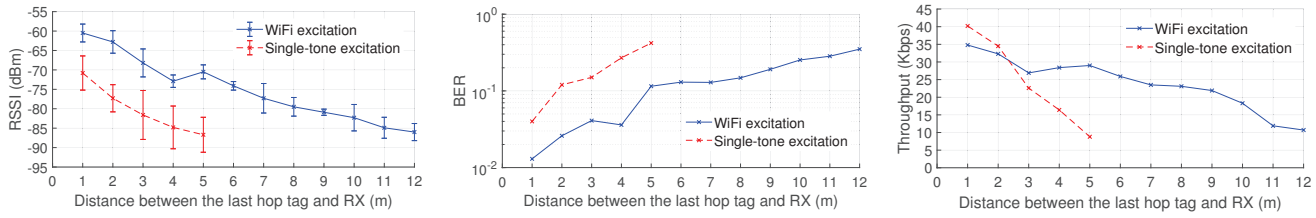

(a) RSSI (b) BER (c) Throughput

Figure 20: DecRel communication performance using digital baseband circuits when the tag-to-tag distance is fixed to 1m: single-tone excitation achieves up to 40Kbps throughput, which is 200x higher than the throughput of X-Tandem.

the single-tone case exceeds that of the WiFi case, it decreases much faster as the last hop distance increases. Figure 20(b) shows that DecRel can achieve a multi-hop throughput of up to 40Kbps with single-tone excitation, which is 200x higher than the throughput of X-Tandem. In addition, single-tone excitation can be used for any hop, while WiFi excitation can only be used for the last hop tag.

Multi-hop backscatter communication range can be defined as the maximum distance between the first hop tag to the reader, which equals to the sum of multiple tag-to-tag distances and the last hop tag-to-reader distance. The communication range of X-Tandem is limited to around 8m, for two reasons. First, X-Tandem tags are non-decodable and only use the first hop excitation, whose transmitter power already decides a coverage. Second, X-Tandem's tag-to-tag distance is up to 0.4m, which is ignorable compared with its last hop distance of up to 8m. Differing from X-Tandem, each tag of the DecRel system can utilize a new excitation signal with good strength, and hence minimize the impact of its previous hop signal strength. This largely improves the tag-to-tag distance. Therefore, DecRel's communication range can be significantly increased as the number of tags increases without a hop count limitation.

4.1.2 Tag-to-tag Distance. This experiment evaluates the impact of DecRel's tag-to-tag distance in the case of two hop backscatter communication. The setup is as follows: The distance between the second hop tag and the reader is set to 1m; We then move the first hop tag away from the second to increase the tag-to-tag distance. We examine the performance including RSSI, BER and throughput with increasing the tag-to-tag distance. To avoid excitation bias, we examine both single-tone excitation and WiFi excitation. Figure 21(a) shows that the average RSSI of the second hop signal nearly has no change when the tag-to-tag distance increases from 1.2m to 4.8m. This result can be expected because each DecRel tag uses its own excitation which is independent of its previous hop excitation. The impact to bit error and throughput is shown in Figure 21(b) and (c). We can see that the second hop tag relay's bit error rate increases and its throughput decreases with increasing the tag-to-tag distance. This is due to the elongated distances from the second hop aggregation node to the two tags. Let D_1 be the distance between the first hop tag and the aggregation node, D_2 be the distance from the aggregation node to the second hop tag, and D_3 be the last hop tag-to-reader distance. Since D_2 is fixed, if tag-to-tag distance increases, D_1 is also increased, which adversely affects BER, throughput and RSSI. The first hop's backscattered signal is first demodulated and then transmitted by the aggregation node to the second hop tag. Here, D_2 impacts the BER of the second hop decoding. The bit errors brought by D_1 and D_2 are imposed on the last hop communication between the second hop tag and the reader, while the increase of D_3 also leads to a worse BER. The following topology configuration should be used to perform the evaluation. The excitation-to-tag distance cannot be longer than 3m, and the aggregation-to-tag distance is up to 1m (due to the limitation of the sensitivity of the envelope detector). The tags and reader are lined up following the route order. The tag-to-tag distance can increase from 1.2m to 4.8m. The last hop tag-to-reader distance can be up to 12m for WiFi excitation and up to 5m for single-tone excitation, respectively. Our measurement data is collected given that all the nodes in this topology are in static positions without mobility. DecRel tags cannot handle the mobility because our current implementation does not involve an on-tag backscatter-based localization mechanism.

4.2 Performance of DecRel with Analog Baseband and Modulation Circuits

We evaluate the performance of analog baseband and modulation circuits. Our results in Figure 22 can be summarized as follows: 1) When the tag-to-tag distance is fixed to 1.6m, the SNR of the last hop signal decreases from about 35dB to about 15dB as the

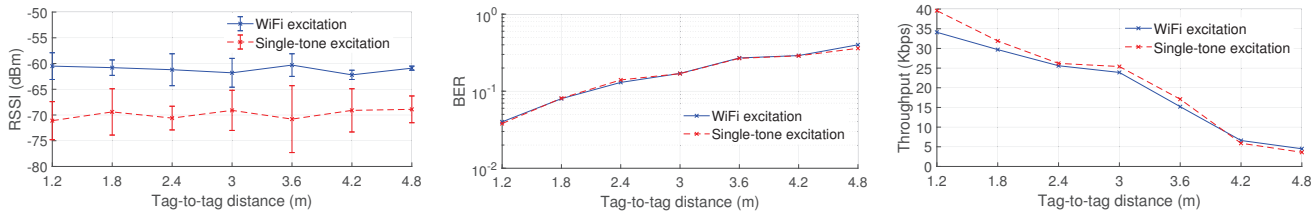

(a) RSSI (b) BER (c) Throughput

Figure 21: Two hop backscatter communication performance across tag-to-tag distance using DecRel's digital baseband circuits when the RX is 1m away from the second hop tag: DecRel does not suffer from multi-hop signal attenuation and its tag-to-tag distance can be up to 4.8m, which is 10x longer than X-Tandem.

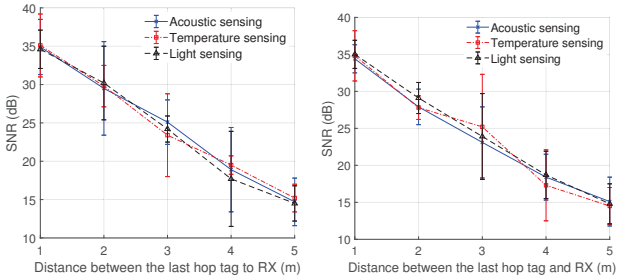

(a) 1.6m tag-to-tag distance (b) 4.8m tag-to-tag distance

Figure 22: The last hop backscattered signal quality of DecRel 48KHz analog baseband and modulation circuits when varying the tag-to-tag distances and the last hop distance: tag-to-tag distance does not impact the last hop SNR for analog signal sensing.

distance between the last hop tag to the reader increases from 1m to 5m; 2) The tag-to-tag distance does not impact the last hop tag-to-reader SNR when it conveys the analog baseband signal of its previous hop tag. This is because the last hop tag uses its own excitation signal, which is independent of previous hop tags and hence experiences little signal attenuation; 3) The three types of sensing circuits achieve similar SNR; 4) DecRel can transmit an audio signal's analog baseband at a 48KHz sample rate, which is equivalent to a bitrate of 768Kbps (if using 16-bit quantization in the reader). As shown in Figure 21(c), the digital baseband achieves a bitrate of up to 40Kbps. Figure 23 shows that the analog baseband and modulation achieve a similar SNR as the digital modes. The analog baseband largely improves the bitrate while it keeps similar SNR as the digital baseband because it uses the PWM signal. Each pulse width symbol conveys richer information (equivalent to to multiple bits) than one bit for a symbol of the digital baseband. In addition, the analog baseband also reduces the power consumption of each tag compared to the digital baseband. This is because it does not use any external sensors or has to implement extra ADC or FPGA drive circuits for the sensors.

4.3 SNR of Simultaneous Sensing and Relay

As introduced in Subsection 2.3, DecRel uses two different frequency shifts to enable simultaneous sensing and relay for a tag. Figure 10 shows the frequency spectrum of the two hop backscatter

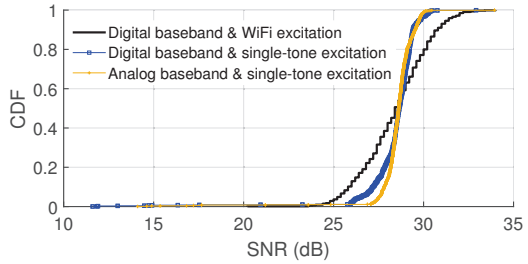

Figure 23: SNR of DecRel using different baseband circuits: baseband type does not impact SNR.

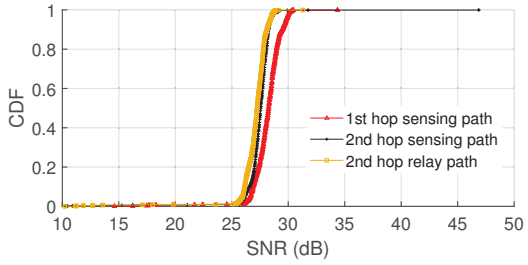

Figure 24: SNR of DecRel when performing simultaneous sensing and relay: multi-hop concurrent communcation does not have interference.

communication. From the frequency-domain result, we can see that there is no interference between the sensing and relaying signals of the second hop tag. We also examine DecRel's sensing and relay by their time-domain signal quality. Figure 24 shows the SNR of simultaneous backscatter communication for the three paths, including the first hop tag's sensing path, the second hop tag's relay path, and the second hop tag's sensing path. The three paths achieve similar SNR, which falls in the range from 25dB to 30dB in almost all the cases.

5 RELATED WORK

Existing relay communication solutions for wireless sensor networks usually employ such commodity technologies as WiFi and Zigbee [43, 44, 62, 63]. Such a network node consists of sensor, microcontroller and RF transceiver, and its decodable forwarding uses coherent demodulation and active transmission, both of which rely on power-consuming high-frequency oscillators. For

example, a WiFi transceiver consumes 0.82~2.10W of power [64]. Compared with the transceiver-based relay, DecRel tag's decoding and backscattering reduce power consumption by eliminating high-frequency oscillators and using analog envelope detection and passive transmission.

Backscatter-based sensors. There has been a significant interest in designing sensors or sensing systems using RFID tags [19, 20, 39–42, 49, 50, 54]. Due to the advances in customized backscatter systems [3-18, 21-38, 51-52], a variety of backscatter-based sensor architectures have been proposed. Ambient backscatter [16] provides a design that enables a batter-free device to sense and communicate with other nearby battery-free devices. Hybrid backscatter [38] is a sensing platform that includes both digital and analog backscatter modulation circuits for audio sensing. EkhoNet [23] presents an ultra low-power sensor architecture using high data rate backscatter. BackFi [6] designs an IoT sensor that can communicate with WiFi devices using backscatter communication. Video streaming backscatter [33] uses analog backscatter technology to enable HD video streaming with a battery-free wireless camera. Differing from previous systems, our work is a sensor architecture that enables simultaneous sensing and relay for multi-hop sensor networks.

Backscatter tag as a receiver. The receiver of backscatter communication can also be a tag that can demodulate the backscattered signal from another tag. Ambient backscatter [16] is the first system that enables a communication path between two tags, where the receiver tag can decode the backscattered signal from the sender tag. Turbocharging ambient backscatter [18] proposes a multi-antenna cancellation design to significantly improve the decoding performance. The backscatter tags in Battery-free cellphone [25] further demodulate voice signals from each other. While a receiver tag is decodable, it does not perform relay communication. This is different from the goal of our tag decoding.

Multi-tag backscatter networks. Efforts have also been made towards backscatter networks. The related works mostly follow the mode that multiple backscatter tags transmit their information concurrently to a reader. FreeRider [26] designs and implements a MAC protocol to assign slots for multi-tag concurrent transmission using Bluetooth and ZigBee excitation. NetScatter [37] demonstrates a network protocol that enables concurrent transmission of 256 backscatter tags with only 500 KHz bandwidth. We consider the network design from a different perspective, which introduces tag relay to expand the scale of a multi-hop backscatter network.

External relay and non-decodable tag relay. There are also relay designs for backscatter networks. RFly [27] is an external relay device that can locate RFID tags and boost their transmission range. X-Tandem [30] uses backscatter tags themself as relays for multi-hop backscatter communication. Our work enables decodable relay in a low-power backscatter tag, while RFly and X-Tandem use analog forwarding without any decoding functions.

6 DISCUSSION AND CONCLUSION

In this paper, we have demonstrated DecRel, a sensor architecture that enables simultaneous sensing and relay for multi-hop backscatter communication. The decodable tag relay and distributed excitation mode significantly enhance the scope and quality of tag relay communication. This is also the first step towards building large-scale low-power sensor mesh networks.

From single-hop to multi-hop. DecRel provides a multi-hop backscatter framework for scalable sensor mesh networking. From hardware design perspective, DecRel tag's decodable relay module is independent of its modulation module, which means DecRel's multi-hop design has potential to incorporate the modulation solutions for a variety of excitation signals in existing single-hop backscatter systems, and to extend them to multi-hop cases. Compared to single-hop backscatter, DecRel's communication range is no longer limited within a tag-to-radio distance but extended to the sum of multiple tag-to-tag distances and a last-hop tag-to-radio distance. This opens up opportunities for distributed backscatter networks with not only long-range transmission but also better connectivity and robustness, to which the tag relay communication will act as a crucial part.

Excitation and aggregation nodes. Our current implementation only supports commodity radio excitation in the last hop. To fully utilize available ambient radios (e.g., smartphones and APs) for each hop, we need to add more complex on-tag decoding functions or a pluggable RFID reader for smartphones [60]. The aggregation node is also possible to be eliminated by integrating a low-power ADC [61] or incorporating the multi-antenna decoding [18] with a trade-off between throughput and tag-to-tag distance.

Multiplexing and concurrent relay requests. If sensing and relaying tasks arrive at the same time, a DecRel tag backscatters their data simultaneously to two different frequencies to avoid interference. This frequency-division approach occupies more frequency spectrum than performing a single type of communication. Time-division multiplexing may save spectral resources, but needs a deliberate design on duty cycle and slot assignment. In addition, for concurrent relay requests, our current implementation uses the control message (Subsection 3.2.3) to notify a tag to process the requests one by one. For large-scale sensor networks, a more efficient way would be to design a network protocol and a tag state machine to coordinate the relay requests.

Tag position detection. We allow a tag to use different forwarding methods according to its mobility and position. Decodable relay is for a long tag-to-tag distance, while non-decodable forwarding can also be used to save energy if a tag moves close to its previous hop's tag and excitation. However, such a selection is not automatic, and our current implementation still needs to send a control message to reconfigure a tag. To enable adaptive tag relay according to mobility, DecRel tags should employ a backscatter-based localization mechanism, e.g., from [27, 35, 36, 53, 54].

7 ACKNOWLEDGMENTS

We would like to thank our shepherd Dr. Aakanksha Chowdhery and the anonymous reviewers for their insightful comments. This work was supported by an Industrial Canada Technology Demonstration Program (TDP) grant, and a Canada NSERC Discovery Grant.

REFERENCES

[1] http://yuneec.uk/index.php/products/h520-uav/h520-craft-uav#h520-copter
[2] https://www.raspberrypi.org/

[3] S. Gollakota, M. S. Reynolds, J. R. Smith, and D. J. Wetherall. The Emergence of RF-Powered Computing. *Computer*, 47(1): 32-39, 2014.

[4] A. Abedi, M. H. Mazaheri, O. Abari, and T. Brecht. WiTAG: Rethinking Backscatter Communication for WiFi Networks. *ACM HotNets*, 2018.

[5] B. Kellogg, A. Parks, S. Gollakota, J. R. Smith, and D. Wetherall. WiFi Backscatter: Internet Connectivity for RF-Powered Devices. *ACM SIGCOMM*, 2014.

[6] D. Bharadia, K. Joshi, M. Kotaru, and S. Katti. BackFi: High Throughput WiFi Backscatter. *ACM SIGCOMM*, 2015.

[7] B. Kellogg, V. Talla, S. Gollakota, and J. R. Smith. Passive Wi-Fi: Bringing Low Power to Wi-Fi Transmissions. *USENIX NSDI*, 2016.

[8] V. Iyer, V. Talla, B. Kellogg, S. Gollakota, and J. R. Smith. Inter-Technology Backscatter: Towards Internet Connectivity for Implanted Devices. *ACM SIGCOMM*, 2016.

[9] P. Zhang, M. Rostami, P. Hu, and D. Ganesan. Enabling Practical Backscatter Communication for On-body Sensors. *ACM SIGCOMM*, 2016.

[10] P. Zhang, D. Bharadia, K. Joshi, and S. Katti. HitchHike: Practical Backscatter Using Commodity WiFi. *ACM SenSys*, 2016.

[11] O. Abari, D. Vasisht, D. Katabi, and A. Chandrakasan. Caraoke: An E-Toll Transponder Network for Smart Cities. *ACM SIGCOMM*, 2015.

[12] J. Gummeson, P. Zhang, and D. Ganesan. Flit: A Bulk Transmission Protocol for RFID-Scale Sensors. *ACM MobiSys*, 2012.

[13] P. Hu, P. Zhang, and D. Ganesan. Laissez-faire: Fully Asymmetric Backscatter Communication. *ACM SIGCOMM*, 2015.

[14] P. Hu, P. Zhang, M. Rostami, and D. Ganesan. Braidio: An Integrated Active-Passive Radio for Mobile Devices with Asymmetric Energy Budgets. *ACM SIGCOMM*, 2016.

[15] B. Kellogg, V. Talla, and S. Gollakota. Bringing Gesture Recognition to All Devices. *USENIX NSDI*, 2014.

[16] V. Liu, A. Parks, V. Talla, S. Gollakota, D. Wetherall, and J. R. Smith. Ambient Backscatter: Wireless Communication Out of Thin Air. *ACM SIGCOMM*, 2013.

[17] V. Liu, V. Talla, and S. Gollakota. Enabling Instantaneous Feedback with Full-Duplex Backscatter. *ACM MobiCom*, 2014.

[18] A. N. Parks, A. Liu, S. Gollakota, and J. R. Smith. Turbocharging Ambient Backscatter Communication. *ACM SIGCOMM*, 2014.

[19] J. Wang, F. Adib, R. Knepper, D. Katabi, and D. Rus. RF-Compass: Robot Object Manipulation Using RFID. *ACM MobiCom*, 2013.

[20] J. Wang, H. Hassanieh, D. Katabi, and P. Indyk. Efficient and Reliable Low-Power Backscatter Networks. *ACM SIGCOMM*, 2012.

[21] P. Zhang and D. Ganesan. Enabling Bit-by-Bit Backscatter Communication in Severe Energy Harvesting Environments. *USENIX NSDI*, 2014.

[22] P. Zhang, J. Gummeson, and D. Ganesan. Blink: A High Throughput Link Layer for Backscatter Communication. *ACM MobiSys*, 2012.

[23] P. Zhang, P. Hu, V. Pasikanti, and D. Ganesan. Ekhonet: High Speed Ultra Low-Power Backscatter for Next Generation Sensors. *ACM MobiCom*, 2014.

[24] A. Wang, V. Iyer, V. Talla, J. R. Smith, and S. Gollakota. FM Backscatter: Enabling Connected Cities and Smart Fabrics. *USENIX NSDI*, 2017.

[25] V. Talla, B. Kellogg, S. Gollakota, and J. R. Smith. Battery-free Cellphone. *ACM UbiComp*, 2017.

[26] P. Zhang, C. Josephson, D. Bharadia, and S. Katti. FreeRider: Backscatter Communication Using Commodity Radios. *ACM CoNEXT*, 2017.

[27] Y. Ma, N. Selby, and F. Adib. Drone Relays for Battery-Free Networks. *ACM SIGCOMM*, 2017.

[28] X. Xu, Y. Shen, J. Yang, C. Xu, G. Shen, G. Chen, and Y. Ni. PassiveVLC: Enabling Practical Visible Light Backscatter Communication for Battery-free IoT Applications. *ACM MobiCom*, 2017.

[29] V. Talla, M. Hassar, B. Kellogg, A. Najafi, J. Smith, and S. Gollakota. LoRa Backscatter: Enabling the Vision of Ubiquitous Connectivity. *ACM Ubicomp*, 2017.

[30] J. Zhao, W. Gong, and J. Liu. X-Tandem: Towards Multi-hop Backscatter Communication with Commodity WiFi. *ACM MobiCom*, 2018.

[31] Y. Peng, L. Shangguan, Y. Hu, Y. Qian, X. Lin, X. Chen, D. Fang, and K. Jamieson. PLoRa: Passive Long-Range Data Networks from Ambient LoRa Transmissions. *ACM SIGCOMM*, 2018.

[32] D. Vasisht, G. Zhang, O. Abari, D. Katabi, H. -M. Lu, and J. Flanz. In-body Backscatter Communication and Localization. *ACM SIGCOMM*, 2018.

[33] S. Naderiparizi, M. Hessar, V. Talla, S. Gollakota, and J. R. Smith. Towards Battery-Free HD Video Streaming. *USENIX NSDI*, 2018.

[34] M. Rostami, J. Gummeson, A. Kiaghadi, and D. Ganesan. Polymorphic Radios: A New Design Paradigm for Ultra-low Power Communication. *ACM SIGCOMM*, 2018.

[35] M. Kotaru, P. Zhang, and S. Katti. Localizing Low-power Backscatter Tags Using Commodity WiFi. *ACM CoNEXT*, 2017.

[36] V. Iyer, R. Nandakumar, A. Wang, S. B. Fuller, and S. Gollakota. Living IoT: A Flying Wireless Platform on Live Insects. *ACM MobiCom*, 2019.

[37] M. Hessar, A. Najafi, and S. Gollakota. NetScatter: Enabling Large-Scale Backscatter Networks. *USENIX NSDI*, 2019.

[38] V. Talla and J. R. Smith. Hybrid analog-digital backscatter: A new approach for battery-free sensing. *IEEE RFID*, 2013.

[39] A. P. Sample, D. J. Yeager, P. S. Powledge, A. V. Mamishev, and J. R. Smith. Design of An RFID-based Battery-free Programmable Sensing Platform. *IEEE Trans. Instrumentation and Measurement*, 57(11): 2608-2615, 2008.

[40] D. J. Yeager, A. P. Sample, and J. R. Smith. Wisp: A Passively Powered UHF RFID Tag with Sensing and Computation. *RFID handbook: Applications, technology, security, and privacy*, (2008): 261-278, 2008.

[41] S. Park, C. Min, and S.-H. Cho. A 95nw Ring Oscillator-based Temperature Sensor for RFID Tags in 0.13 um CMOS. *IEEE International Symposium on Circuits and Systems (ISCAS)*, 2009.

[42] S. Roy, V. Jandhyala, J. Smith, D. Wetherall, B. Otis, R. Chakraborty, M. Buettner, D. Yeager, Y.-C. Ko, and A. Sample. RFID: From Supply Chains to Sensor Nets. *Proceedings of the IEEE*, 98(9): 1583-1592, 2010.

[43] S. Katti, D. Katabi, H. Balakrishnan, and M. Medard. Symbol-level Network Coding for Wireless Mesh Networks. *ACM SIGCOMM*, 2008.

[44] O. Gnawali, R. Fonseca, K. Jamieson, D. Moss, and P. Levis. Collection Tree Protocol. *ACM SenSys*, 2009.

[45] W. R. Heinzelman, J. Kulik, and H. Balakrishnan. Adaptive Protocols for Information Dissemination in Wireless Sensor Networks. *ACM MobiCom*, 1999.

[46] M. Zorzi and R. R. Rao. Geographic Random Forwarding (GeRaF) for Ad Hoc and Sensor Networks: Energy and Latency Performance. *IEEE Trans. Mobile Computing*, 2(4): 349-365, 2003.

[47] S. Roundy, P. K. Wright, and J. Rabaey. A Study of Low Level Vibrations as A Power Source for Wireless Sensor Nodes. *ELSEVIER Computer Communications*, 26(11): 1131-1144, 2003.

[48] J. Polastre, J. Hill, and D. Culler. Versatile Low Power Media Access for Wireless Sensor Networks. *ACM SenSys*, 2004.

[49] S. Johan, X. Zeng, T. Unander, A. Koptyug, and H.-E. Nilsson. Remote Moisture Sensing Utilizing Ordinary RFID Tags. *IEEE Sensors*, 2007.

[50] R. Bhattacharyya, C. Floerkemeier, and S. Sarma. Low-cost, Ubiquitous RFID-tag-antenna-based Sensing. *Proceedings of the IEEE*, 98(9):1593-1600, 2010.

[51] J.F. Ensworth and M.S. Reynolds. Every Smart Phone Is A Backscatter Reader: Modulated Backscatter Compatibility with Bluetooth 4.0 Low Energy (BLE) Devices. *IEEE RFID*, 2015.

[52] R. Zhao, F. Zhu, S. Peng, Y. Feng, X. Tian, H. Yu, and X. Wang. OFDMA-Enabled Wi-Fi Backscatter. *ACM MobiCom*, 2019.

[53] L. Yang, Y. Chen, X. Li, C. Xiao, Mo Li, and Y. Liu. Tagoram: Real-Time Tracking of Mobile RFID Tags to High Precision Using COTS Devices. *ACM MobiCom*, 2014.

[54] Z. Luo, Q. Zhang, Y. Ma, M. Singh, and F. Adib. 3D Backscatter Localization for Fine-Grained Robotics. *USENIX NSDI*, 2019.

[55] J. Jang and F. Adib. Underwater Backscatter Networking. *ACM SIGCOMM*, 2019.

[56] https://www.msoon.com/lvpm-software-download

[57] https://www.cadence.com/en_US/home/tools/custom-ic-analog-rf-design/circuit-design.html

[58] https://www.tsmc.com/english/dedicatedFoundry/technology/logic.htm#l_65nm_technology

[59] https://www.xilinx.com/products/design-tools/xst.html

[60] http://www.rfidtagworld.com/products/Ear-Jack-reader-UHF_1056.html

[61] M. Eslami, M. Taherzadeh-Sani, and F. Nabki. A 1-V 690μw 8-bit 200 MS/s Flash-SAR ADC with Pipelined Operation of Flash and SAR ADCs in 0.13μm CMOS. *IEEE International Symposium on Circuits and Systems*, 2015.

[62] L. Li, H. Xiaoguang, C. Ke and H. Ketai. The Applications of WiFi-based Wireless Sensor Network in Internet of Things and Smart Grid. *IEEE Conference on Industrial Electronics and Applications*, 2011.

[63] C. Zhang, X. Zhang, and R. Chandra. Energy Efficient WiFi Display. *ACM MobiSys*, 2015.

[64] D. Halperin, B. Greenstein, A. Sheth, and D. Wetherall. Demystifying 802.11n Power Consumption. *ACM HotPower*, 2010.